Virtual Corrosion Initiation Monitoring for Infrastructures Considering Environmental Uncertainty

Yuguo Yu
Centre for Infrastructure Engineering and Safety, School of Civil and Environmental Engineering, The University of New South Wales, Sydney, NSW 2052, Australia Email: yuguo.yu@unsw.edu.au

Wei Gao
Centre for Infrastructure Engineering and Safety, School of Civil and Environmental Engineering, The University of New South Wales, Sydney, NSW 2052, Australia Email: w.gao@unsw.edu.au

Qihan Wang
Centre for Infrastructure Engineering and Safety, School of Civil and Environmental Engineering, The University of New South Wales, Sydney, NSW 2052, Australia Email: qihan.wang@unsw.edu.au

Bin Dong
Centre for Infrastructure Engineering and Safety, School of Civil and Environmental Engineering, The University of New South Wales, Sydney, NSW 2052, Australia Email: bin.dong@unsw.edu.au

Abstract: Material decay and corrosion of reinforced concrete infrastructures have long been recognized as major damage indicators in modern structural health monitoring. In order to further transform from reactive monitoring to proactive prediction and risk prevention, the key resides in the developments of high-fidelity physics-based modelling method to generate robust prior estimates considering uncertainty. To this end, this paper is concerned with a novel metamodeling on the chloride-induced corrosion initiation of reinforced concrete infrastructures. The physics-based modelling of uncertain material decay represents a chemophysical process, involving various coupling effects and environmental uncertainties, leading to a complex stochastic system that requires computational-heavy approaches to generate useful statistical analyses. In this regard, the computational intensiveness is addressed by the recently reported extended support vector regression (X-SVR) method. The advanced performance of the proposed approach is explored by modelling a real-life reinforced concrete parking infrastructure.

Keywords: Chemophysical modelling; Degradation; Machine learning; Virtual corrosion monitoring

1. Introduction

Structural health is concerned with the probabilistic responses of materials and structures in widespread areas. In civil engineering, one major durability concern is the reinforcement corrosion (Panesar and Ching 2018), which is found in concrete infrastructures subjected to environmental decays. The mechanism of corrosion initiation is known to be caused by the penetration and the accumulation of chloride (Muthulingam and Rao 2014, Hornbostel et al. 2016, Jin et al. 2018). However, many uncertain factors could substantially complicate the detailed assessment (Ann and Song 2007).

This paper deals with the virtual corrosion monitoring on the probabilistic corrosion initiation of a real-life parking infrastructure under the seasonal application of de-icing salt. Most of the reported studies on this issue were deterministic thus far (Samson and Marchand 2007), and simplifications on the degradation models were heavily used in the reported probabilistic studies (Hackl and Kohler 2016, Li and Ye 2018, Zhang 2018). In durability assessment, most of the models for chloride ingress were based on the Fick's law and prescribed binding isotherms, where many coupling effects were ignored. As a result, the low fidelity of the reported methods in the real-life scenarios is suspected to generate only poor estimates.

The technical difficulties hindering the comprehensive durability analysis under uncertainty are twofold. First, modelling the material decay represents a chemophysical problem (Yu et al. 2015, Yu and Zhang 2017, Yu and Zhang 2018, Yu and Zhang 2018, Yu et al. 2019), where the analysis under uncertainty involves solving stochastic partial differential equations (SPDEs) of multi-species transportation coupled with algebraic equations for chemical reactions. In order to achieve a informed statistical analysis, solving such a complex system often requires exhausting Monte Carlo simulations (MCS) (Yu et al. 2018). The computational intensiveness thus becomes a major concern, which represents the second difficulty. To address these issues, the metamodeling method combining machine learning with the stochastic chemophysical modelling of corrosion initiation is exploited in this paper.

In the following context, the developments of the novel machine learning algorithm and the stochastic chemophysical finite element analysis are presented. Focusing on the virtual corrosion monitoring of reinforced concrete infrastructure subjected to seasonal applications of de-icing salt, the details of the stochastic chemophysical models are presented in Section 2. The recently reported machine learning algorithm, i.e. the extended support vector regression (X-SVR), is then presented in Section 3. The effectiveness and efficiency of performing the machine learning aided corrosion initiation analysis is explored in Section 4, with some concluding remarks presented in Section 5.

2. Modelling chloride-induced corrosion initiation

To conduct high-fidelity corrosion initiation monitoring, a variety of chemical reactions associated with the hydrated cement system must by innovatively incorporated. Firstly, to reduce computational cost, the operator splitting approach (OSA) is implemented, and chemical reactions are evaluated by the thermodynamic modelling method (Yu et al. 2015). Herein, the general format of chemical equilibrium model following thermodynamic modelling is given below, where the details regarding the complete set of chemical reactions as considered in the modelled were reported in (Yu et al. 2019).

$$K_m = \prod_i [u_i]^{\nu_{i,m}} \gamma_i^{\nu_{i,m}} \Big/ \prod_j [u_j]^{\nu_{j,m}} \gamma_j^{\nu_{j,m}},\ m \in [1, M] \tag{1}$$

where K_m is equilibrium constant (-) for the *m*th reaction, $[u_i], \gamma_i, \nu_i$ and $[u_j], \gamma_j, \nu_j$ are concentration (M), activity coefficient (-) and valence number (-) of the *i*th product and the *j*th reactant respectively.

Furthermore, in addition to the general chemical equilibrium of the hydrated cement system, the most crucial impact to be considered in virtual corrosion monitoring is the chloride binding effect during exposure. Herein, the chloride binding is modelled in detail by differentiating the binding mechanism, i.e.,

physical and chemical bindings. In specific, physical binding describes the ionic exchange between the free ionic chloride and the hydroxyl group at the electrical double layer of the C-S-H gel. The free chloride is physically attached to the binding sites without creating new compounds, hence the physical binding.

$$\underbrace{\left[\text{C-S-H}-\text{OH}^-\right]}_{\text{C-S-H gel}}+\text{Na}^++\text{Cl}^-\rightleftarrows\underbrace{\left[\text{C-S-H}-\text{Cl}^-\right]}_{\text{C-S-H gel}}+\text{Na}^++\text{OH}^- \tag{2}$$

Following the double layer theory (Pan et al. 2010), the physical chloride binding is calculated as:

$$c_b^{\text{phy}}=\frac{\text{A}_\text{s}\text{N}_\text{s}K_{\text{phy}}\left[\text{Cl}^-\right]}{\left[\text{OH}^-\right]+K_{\text{phy}}\left[\text{Cl}^-\right]}N_{\text{C-S-H}} \tag{3}$$

where N_s is total binding capacity (mol/m^2) on the C-S-H surface, which is reported to be $1.793\times10^{-7}\,\text{mol}/\text{m}^2$ (Pan et al. 2010), K_{phy} is physical binding coefficient (-), reported to be 0.0698 (Baroghel-Bouny et al. 2012), A_s is surface area of the C-S-H gel ($250916\,\text{m}^2/\text{mol}$ of the C-S-H gel), $N_{\text{C-S-H}}$ is remaining solid content of the C-S-H gel ($\text{mol}/\text{m}^3=\text{mmol}/\text{L}$ of the material), and c_b^{phy} is amount of (mmol/L of material) physically-bound chloride content.

On the other hand, chemical binding indicates the reaction between free ionic chloride and monosulfate, leading to the formations of new compounds. The chemical binding is generally attributed to the formation of the Friedel's salt due to its dominant amount (Baroghel-Bouny et al. 2012).

$$\underbrace{\left[\text{AFm}-\text{SO}_4^{2-}\right]}_{\text{Monosulfate}}+2\text{Cl}^-\rightleftarrows\underbrace{\left[\text{AFm}-2\text{Cl}^-\right]}_{\text{Friedel's salt}}+\text{SO}_4^{2-} \tag{4}$$

Unlike the dissolution of Friedel's salt modelled as a part of the AFm solid solution, the formation of Friedel's salt follows another ionic exchange (Lito et al. 2012), and is calculated as:

$$c_b^{\text{che}}=\frac{2\times K_{\text{che}}\left\{\text{Cl}^-\right\}^2}{\left\{\text{SO}_4^{2\text{-}}\right\}+K_{\text{che}}\left\{\text{Cl}^-\right\}^2}N_{\text{AFm}} \tag{5}$$

where {...} indicates activity of diffusive reactant (mol/L of solution), K_{che} is equilibrium coefficient for ionic exchange, assumed to be 0.1 at 23°C (Bothe and Brown 2004), N_{AFm} (mmol/L of material) represents the remaining amount of AFm solid solution that is occupied by Friedel's salt and monosulfate, and c_b^{che} is amount (mmol/L of material) of the chemically-bound chloride content.

The ionic exchange of chloride binding would result in retardation of chloride ingress, which should be included in the reactant transportation. To do so, the derivatives of ionic exchange are calculated:

$$\frac{\partial c_b^{\text{phy}}}{\partial c_{\text{f}}}=\frac{\partial c_b^{\text{phy}}}{\partial\left[\text{Cl}^-\right]}=\frac{\text{A}_{\text{s}}\text{N}_{\text{s}}K_{\text{phy}}\left[\text{OH}^-\right]}{\left(\left[\text{OH}^-\right]+K_{\text{phy}}\left[\text{Cl}^-\right]\right)^2}N_{\text{C-S-H}}\ \text{and}\ \frac{\partial c_b^{\text{che}}}{\partial c_{\text{f}}}=\frac{\partial c_b^{\text{che}}}{\partial\left[\text{Cl}^-\right]}=\frac{4\times K_{\text{che}}\gamma_{\text{Cl}}^2\left[\text{Cl}^-\right]\left\{\text{SO}_4^{2-}\right\}}{\left(\left\{\text{SO}_4^{2-}\right\}+K_{\text{che}}\left\{\text{Cl}^-\right\}^2\right)^2}N_{\text{AFm}} \quad (6)$$

By doing so, the stochastic Nernst-Planck equation for chloride penetration is formulated as follow:

$$\left(\frac{\partial c_b^{\text{phy}}}{\partial c_{\text{f}}}+\frac{\partial c_b^{\text{che}}}{\partial c_{\text{f}}}\right)\frac{\partial c_{\text{f}}}{\partial t}+\frac{\partial w_{\text{L}}c_{\text{f}}}{\partial t}=\text{div}\left[\begin{array}{l}\boldsymbol{D}_{\text{f}}w_{\text{L}}\text{grad}(c_{\text{f}})+\dfrac{\boldsymbol{D}_{\text{f}}\mathbf{z}\text{F}}{\text{R}T}c_{\text{f}}\text{grad}(\psi)+\boldsymbol{D}_{\text{f}}w_{\text{L}}c_{\text{f}}\text{grad}(\ln\gamma)\\+\dfrac{\boldsymbol{D}_{\text{f}}c_{\text{f}}\ln(\gamma c_{\text{f}})}{T}\text{grad}(T)+c_{\text{f}}\boldsymbol{D}_{\text{L}}\text{grad}(RH)\end{array}\right]+Q_{\hat{U}}\frac{\partial\boldsymbol{W}_{\hat{U}}}{\partial t} \quad (7)$$

where w_{L} is volumetric liquid content (m^3/m^3), $\mathbf{z}$ is valence number of the diffusive reactant (-), F is Faraday constant (96488.46C/mol), R is ideal gas constant (8.3143J/mol/K), T is thermodynamic temperature (K), ψ is electrical potential (V), γ is chemical activity coefficient (-), $\boldsymbol{D}$ is diffusivity vector (m^2/s), RH is relative humidity (%). In addition, $Q_{\hat{U}}\partial\boldsymbol{W}_{\hat{U}}$ are the noise terms, and $Q_{\hat{U}}$ is the covariance relying on the solutions to diffusive reactants, chemical reactions, and other coupling effects.

3. Extended support vector regression (X-SVR)

To achieve stochastic analyses with acceptable accuracy, the scale of the MCS often ranges from 10000 to a couple of millions. Thus, machine learning based methods, as a surrogate model (Ben Abdessalem and El-Hami 2015), become a popular solution to mitigate computational intensiveness. Herein, a recently developed support vector regression (SVR) algorithm is introduced, which was extended from the doubly regularised SVM (DrSVM) for binary classification to regression (Dunbar et al. 2010, Li et al. 2016), hence the extended support vector regression (X-SVR).

In X-SVR, instead of using the linear ε-insensitive loss function as in the conventional ε-SVR (Smola and Schölkopf 2004), a quadratic ε-insensitive loss function (l_2^{ε}) is adopted.

$$l_2^{\varepsilon}(y_{train}^i-\hat{f}(\mathbf{x}_i))=\left|y_{train}^i-\hat{f}(\mathbf{x}_i)\right|^2,i=1,...m \quad (8)$$

where $\mathbf{x}$ and $\mathbf{y}_{train}\in\Re^m$ are the input vector and response from the available knowledge, i.e. the training dataset, $\hat{f}(\mathbf{x}_i)$ indicates surrogate model prediction.

Although applying the quadratic ε-insensitive loss function enhances the numerical stability in X-SVR, the algorithm may still struggle to model problems of high nonlinearity. In the present case of predicting the stochastic corrosion initiation, the multi-physical problem and the associated uncertainty would lead to a highly nonlinear regression. Under this circumstance, a surrogate model may not be found directly based on

the input features, and further processing on $\mathbf{x}_{train}$ is required. To do so, it is achieved by mapping raw input data from the low-dimensional space $\Re^n$ into a higher-dimensional feature space F with an empirical mapping function $\mathbf{\Phi}(\mathbf{x}_i)$ (Kung 2014). Such an approach leads to the development of a kernelized X-SVR.

$$\mathbf{x}_i = [x_{i,1}, x_{i,2}, ..., x_{i,n}]^T \mapsto \hat{\mathbf{k}}(\mathbf{x}_i) = \begin{bmatrix} \mathbf{\Phi}(\mathbf{x}_1)^T \mathbf{\Phi}(\mathbf{x}_i) \\ \mathbf{\Phi}(\mathbf{x}_2)^T \mathbf{\Phi}(\mathbf{x}_i) \\ \vdots \\ \mathbf{\Phi}(\mathbf{x}_m)^T \mathbf{\Phi}(\mathbf{x}_i) \end{bmatrix} = \begin{bmatrix} K(\mathbf{x}_1, \mathbf{x}_i) \\ K(\mathbf{x}_2, \mathbf{x}_i) \\ \vdots \\ K(\mathbf{x}_m, \mathbf{x}_i) \end{bmatrix} \tag{9}$$

Through kernel mapping, the empirical feature vector $\hat{\mathbf{k}}(\mathbf{x}_i)$ is regarded as training samples, and the surrogate model generated from kernelized X-SVR model is derived by solving the constrained optimization problem as follow:

$$\min_{\mathbf{z}_k, \gamma} : \frac{1}{2}(\mathbf{z}_k^T \hat{\mathbf{C}}_k \mathbf{z}_k + \gamma^2) + \lambda_2 \mathbf{b}_k^T \mathbf{z}_k \quad s.t. \quad (\hat{\mathbf{A}}_k + \mathbf{I}_{4m\times 4m})\mathbf{z}_k + (\varepsilon \mathbf{I}_{4m\times 4m} + \gamma \hat{\mathbf{G}}_k)\hat{\mathbf{e}}_k + \hat{\mathbf{d}}_k \geq \mathbf{0}_{4m} \tag{10}$$

where $\mathbf{I}_{4m\times 4m} \in \Re^{4m\times 4m}$ and $\mathbf{0}_{4m} \in \Re^{4m}$ denote the identity matrix and the zero vector. The matrices $\hat{\mathbf{C}}_k$, $\hat{\mathbf{G}}_k$ and $\hat{\mathbf{A}}_k$, as well as the vectors $\mathbf{b}_k$, $\hat{\mathbf{e}}_k$, $\hat{\mathbf{d}}_k$ and $\mathbf{z}_k$ were carefully defined in (Yu et al. 2019). More importantly, the proof that the X-SVR would lead to global optimum solution have also been discussed intensively by (Yu et al. 2019).

4. Results and analyses

The performance of the proposed method is examined here by studying the real-life case as found in a 20-year-old concrete parking structure (Samson and Marchand 2007). The structure was in Canada, where the harsh winter led to seasonal adoption of de-icing salt.

The concrete material of the parking structure is reported to be made of the CSA Type-10 ordinary Portland cement with a *w*/*b* ratio of 0.45. The detailed material properties, such as hydrate contents, solution composition, microstructure and thermal conductivity, are referred to the reported study (Samson and Marchand 2007). The physical monitoring was conducted by measuring the chloride profile in the core samples extracted from the slab after 20-year exposure. A schematic diagram describing the field corrosion initiation monitoring is presented in the Figure 1.

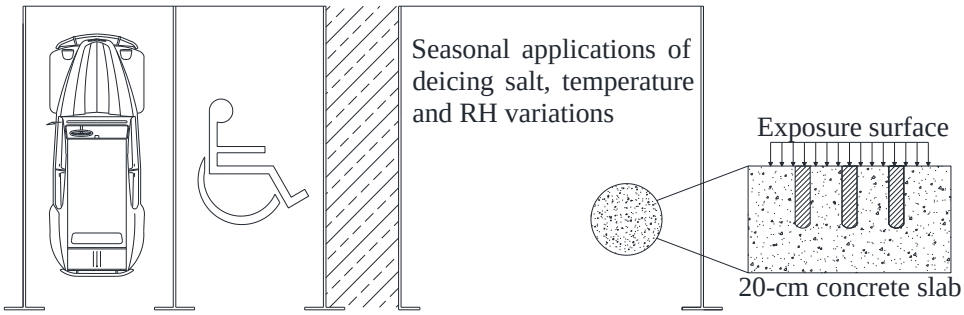

Figure 1. Schematic diagram of physical corrosion monitoring on a parking infrastructure

Since field structure is bound to interact with environment, the representations of boundary conditions are the decisive factor for the accurate virtual monitoring. According to (Samson and Marchand 2007), the data as collected from the local weather station reflecting the annual variations of temperature, RH and surface concentration of de-icing salt are adopted to represent the in-situ boundary conditions, see Figure 2.

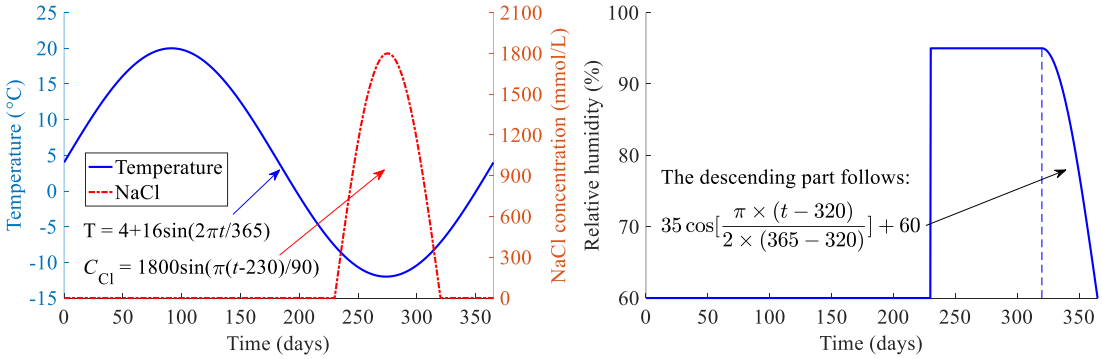

Figure 2. Annual variations in the boundary conditions: (a) temperature and NaCl; (b) RH

Considering the variations in environmental conditions, the associated uncertainties are thus assigned to the peak dosage of de-icing salt ($C^R_{\mathrm{Cl}_{\max}}$), annual average temperature (T^R_{ave}) and relative humidity (RH^R_{ave}). The assumed statistical representations for environmental uncertainties are summarised in the Table I.

Table I. Random parameters for the durability assessment

Variables	Mean	COV	Distribution type
RH^R_{ave}	60%	0.03	Lognormal
T^R_{ave}	$4\,^{\circ}C$	0.05	Normal
$C^R_{\mathrm{Cl}_{\max}}$	$1800\,\mathrm{mmol/L}$	0.056	Uniform

The full-scale MCS (1000,000 function evaluations) using the stochastic chemophysical model is conducted first. The modelling of the long-term chloride ingress involves of a 20-year seasonal exposure of concrete to the de-icing salt. The MCS results are obtained for the chloride profiles at Year 5, 10, 15 and 20

to demonstrate the chloride ingress process and the uncertainty propagation. In addition, the field measurements after the 20-year exposure are also presented for inspection.

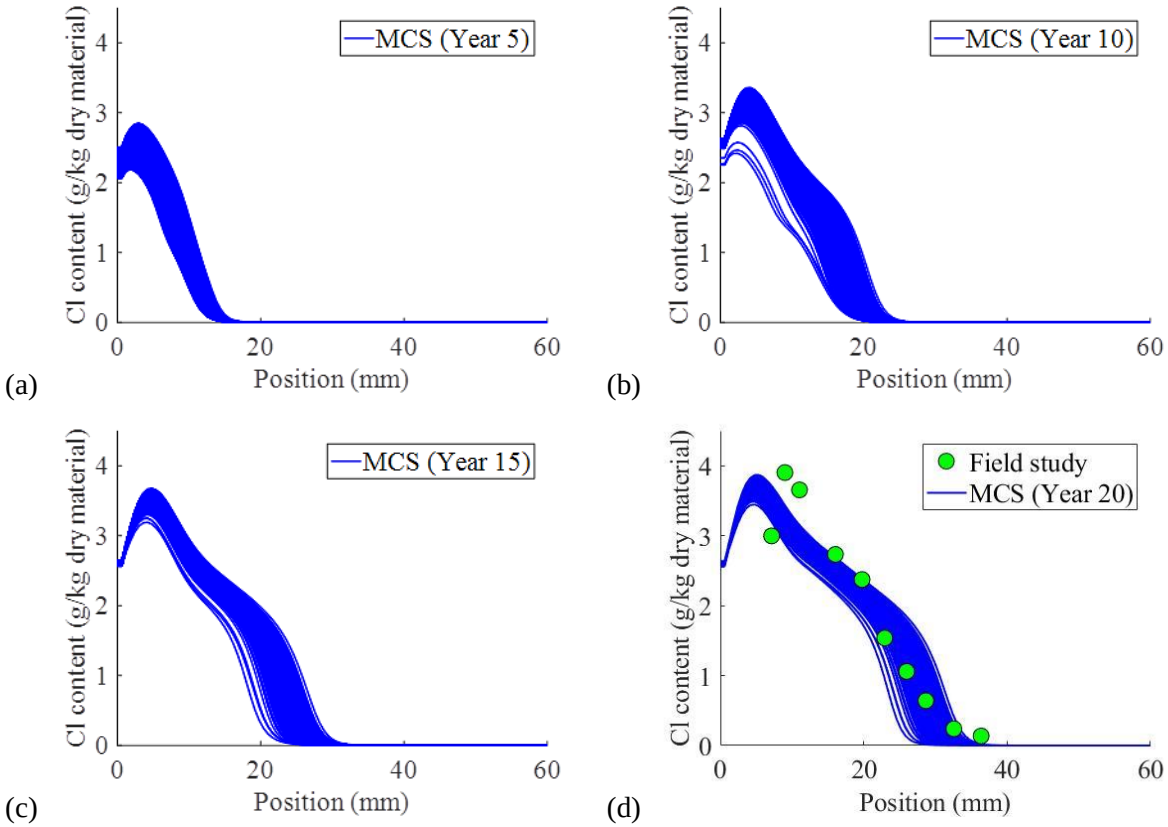

Figure 3. Comparisons between the full-scale MCS and the field measurement

Examining *Figure 3*, near the exposure surface, the chloride profile experiences a localized peak due to the strong advection effect. However, this peak of chloride content is not critical for assessing corrosion initiation. Instead, the chloride content at the reinforcement surface are the main focuses. Herein, both ε-SVR and X-SVR are implemented with a Gaussian kernel. The number of training samples used for deriving the surrogate model is set to be 50, and the obtained results are compared to the full-scale MCS. Specifically, by assuming the cover depth of 20mm and 25mm for a typical slab structure as adopted in public parking infrastructure, the chloride content at the reinforcement surface at Year 10 and 20 are examined, see the Figures 4-7.

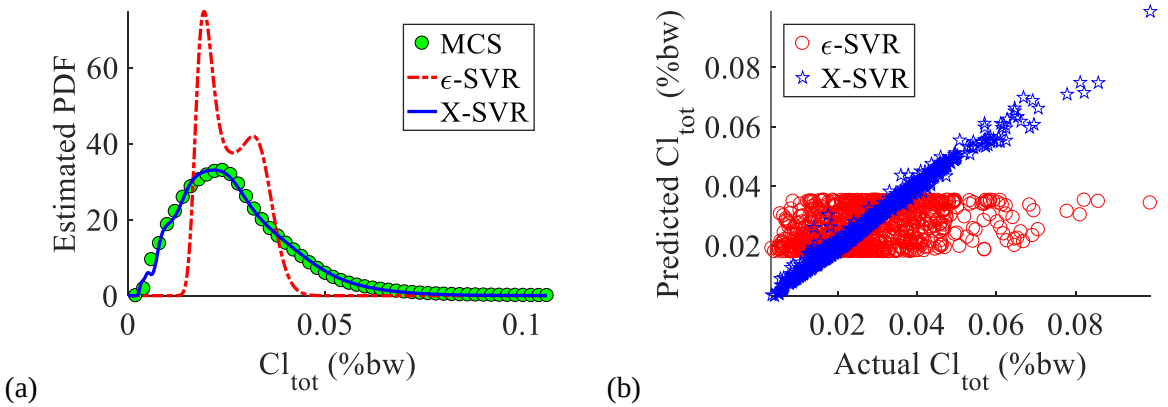

Figure 4. Total chloride content at the presumed concrete cover of 20mm after 10-year exposure

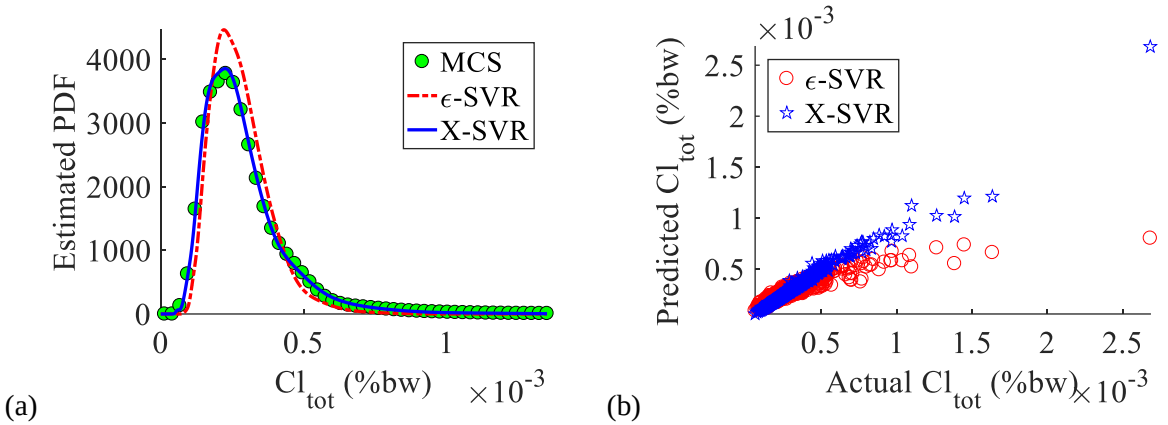

Figure 5. Total chloride content at the presumed concrete cover of 25mm after 10-year exposure

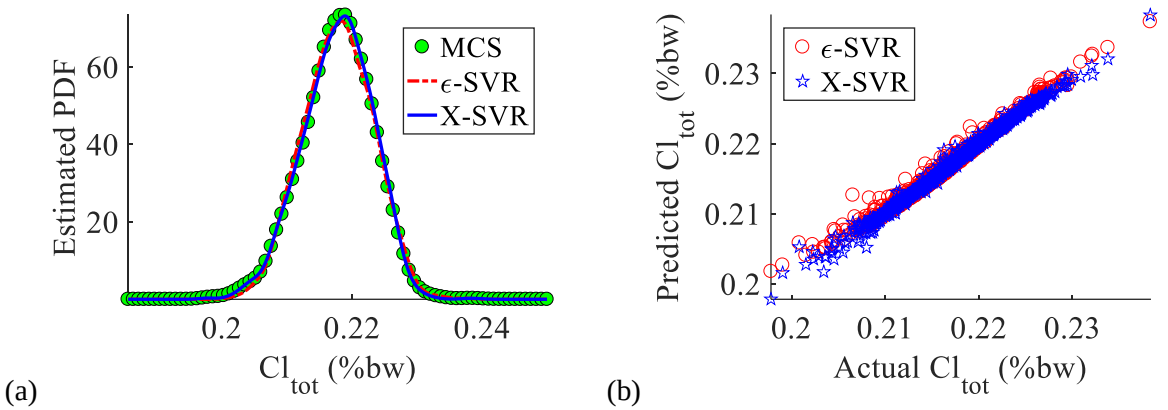

Figure 6. Total chloride content at the presumed concrete cover of 20mm after 20-year exposure

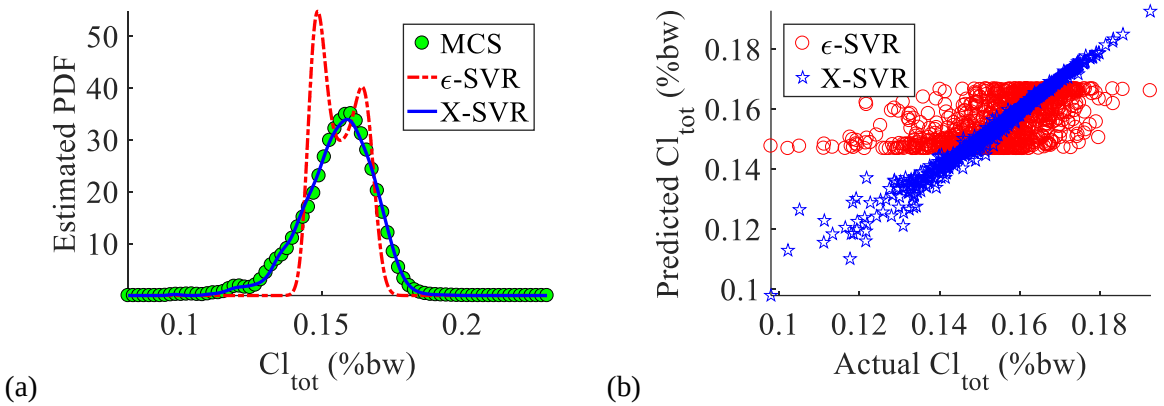

Figure 7. Total chloride content at the presumed concrete cover of 25mm after 20-year exposure

For surrogate modelling the chloride content at the cover depth, the conventional ε-SVR experiences more difficulty in precisely predicting the full-scale MCS. This is mainly due to the complex and nonlinear chemophysical mechanisms regarding the chloride transportation in a real-life case. As discussed in the previous sections, many interrelated factors would affect the overall transportation process. For instance, the changing boundaries would affect diffusivity, reactivity and moisture movement, leading to different paces in terms of the progressive degradation. The uncertain material decay process leads to more detailed differences as found in hydrate compositions, hence different chloride binding capacity and chloride penetration degrees in general. Furthermore, the distinct pace in the microstructural evolutions also brings contrasts to the material diffusivity and permeability. All these variations would cause interrelated influences within the chemophysical modelling. As a result, obtaining accurate correlation between chloride accumulation at the reinforcement surface and the uncertain environmental input indicates a complex regression problem for surrogate modelling, which is governed by the complex chemophysical process of high nonlinearity. As shown in the above figures, by using a low number of actual function evaluations, the X-SVR generates good predictions on the total chloride content regardless of cover depth and in-service duration. In comparison, the ε-SVR fails to generate meaningful predictions in multiple occasions.

5. Summary

Excellent performances of the recently developed X-SVR are demonstrated to be an effective and efficient surrogate modelling approach for the physics-based virtual monitoring of corrosion initiation considering environmental uncertainties. The X-SVR well predicts the total chloride accumulation at the reinforcement surface with low function evaluations required. i.e. training samples. In comparison, the performance of ε-SVR is inconsistent, which often fails to generate meaningful estimations on the stochastic responses.

Acknowledgements

This research work presented has been supported by Australian Research Council project IH150100006. The presented numerical computations are undertaken with the assistance of resources and services from the National Computational Infrastructure (NCI), which is supported by the Australian Government.

References

Ann, K. Y. and H.-W. Song. Chloride threshold level for corrosion of steel in concrete. Corrosion Science, 49(11): 4113-4133, 2007.

Baroghel-Bouny, V., X. Wang, M. Thiery, M. Saillio and F. Barberon. Prediction of chloride binding isotherms of cementitious materials by analytical model or numerical inverse analysis. Cement and Concrete Research, 42(9): 1207-1224, 2012.

Ben Abdessalem, A. and A. El-Hami. A probabilistic approach for optimising hydroformed structures using local surrogate models to control failures. International Journal of Mechanical Sciences, 96-97(143-162, 2015.

Bothe, J. V. and P. W. Brown. PhreeqC modeling of Friedel's salt equilibria at 23±1 °C. Cement and Concrete Research, 34(6): 1057-1063, 2004.

Dunbar, M., J. M. Murray, L. A. Cysique, B. J. Brew and V. Jeyakumar. Simultaneous classification and feature selection via convex quadratic programming with application to HIV-associated neurocognitive disorder assessment. European Journal of Operational Research, 206(2): 470-478, 2010.

Hackl, J. and J. Kohler. Reliability assessment of deteriorating reinforced concrete structures by representing the coupled effect of corrosion initiation and progression by Bayesian networks. Structural Safety, 62(12-23, 2016.

Hornbostel, K., U. M. Angst, B. Elsener, C. K. Larsen and M. R. Geiker. Influence of mortar resistivity on the rate-limiting step of chloride-induced macro-cell corrosion of reinforcing steel. Corrosion Science, 110(46-56, 2016.

Jin, M., S. Gao, L. Jiang, H. Chu, M. Lu and F. F. Zhi. Degradation of concrete with addition of mineral admixture due to free chloride ion penetration under the effect of carbonation. Corrosion Science, 138(42-53, 2018.

Kung, S. Y. (2014). Kernel methods and machine learning. United Kingdom, Cambridge University Press.

Li, J., Y. Wang, Y. Cao and C. Xu. Weighted doubly regularized support vector machine and its application to microarray classification with noise. Neurocomputing, 173(595-605, 2016.

Li, Q. and X. Ye. Surface deterioration analysis for probabilistic durability design of RC structures in marine environment. Structural Safety, 75(13-23, 2018.

Lito, P. F., S. P. Cardoso, J. M. Loureiro and C. M. Silva (2012). Ion Exchange Equilibria and Kinetics. Ion Exchange Technology I: Theory and Materials. I. Dr and M. Luqman. Dordrecht, Springer Netherlands: 51-120.

Muthulingam, S. and B. N. Rao. Non-uniform time-to-corrosion initiation in steel reinforced concrete under chloride environment. Corrosion Science, 82(304-315, 2014.

Pan, T., K. Xia and L. Wang. Chloride binding to calcium silicate hydrates (C-S-H) in cement paste: a molecular dynamics analysis. International Journal of Pavement Engineering, 11(5): 367-379, 2010.

Panesar, D. K. and G.-H. Ching. Implications of coupled degradation mechanisms of cement based materials exposed to cold climates. International Journal of Mechanical Sciences, 144(865-876, 2018.

Samson, E. and J. Marchand. Modeling the effect of temperature on ionic transport in cementitious materials. Cement and Concrete Research, 37(3): 455-468, 2007.

Smola, A. J. and B. Schölkopf. A tutorial on support vector regression. Statistics and Computing, 14(3): 199-222, 2004.

Yu, Y., X. Chen, W. Gao, Q. Li, D. Wu and M. Liu. Stochastic leaching analysis on cementitious materials considering the influence of material uncertainty. Construction and Building Materials, 184(186-202, 2018.

Yu, Y., X. Chen, W. Gao, D. Wu and A. Castel. Impact of atmospheric marine environment on cementitious materials. Corrosion Science, 148(366-378, 2019.

Yu, Y., D. Wu, Q. Wang, X. Chen and W. Gao. Machine learning aided durability and safety analyses on cementitious composites and structures. International Journal of Mechanical Sciences, 160(165-181, 2019.

Yu, Y. and Y. X. Zhang. Coupling of chemical kinetics and thermodynamics for simulations of leaching of cement paste in ammonium nitrate solution. Cement and Concrete Research, 95(95-107, 2017.

Yu, Y. and Y. X. Zhang. Effect of capillary connectivity and crack density on the diffusivity of cementitious materials. International Journal of Mechanical Sciences, 144(849-857, 2018.

Yu, Y. and Y. X. Zhang. Numerical modelling of mechanical deterioration of cement mortar under external sulfate attack. Construction and Building Materials, 158(490-502, 2018.

Yu, Y., Y. X. Zhang and A. Khennane. Numerical modelling of degradation of cement-based materials under leaching and external sulfate attack. Computers & Structures, 158(1-14, 2015.

Zhang, H. Durability reliability analysis for corroding concrete structures under uncertainty. Mechanical Systems and Signal Processing, 101(26-37, 2018.